Flexible Robotic Scanning Device for Intraoperative Endomicroscopy in MIS

Siyang Zuo, Michael Hughes, and Guang-Zhong Yang, *Fellow, IEEE*

***Abstract*—Optical biopsy methods such as probe-based confocal endomicroscopy can provide intraoperative real-time assessment of tumour margins, including during minimally invasive surgery with flexible endoscopes or robotic platforms. Mosaics can be produced by translating the probe across the target, but it remains difficult to scan over a large field-of-view with a flexible endomicroscope. In this paper, we have developed a novel flexible scanning device for intraoperative endomicroscopy in MIS. A Schott leached imaging bundle was integrated into the device and enables the approach, via a flexible path, to deep and narrow spaces in the human body that otherwise would not accessible. The proposed device uses a gear-based flexible concentric tube scanning mechanism to facilitate large field-of-view mosaicing. Experimental results show that the device is able to scan different surface trajectories (e.g. a spiral pattern over a hemi-spherical surface). Results from lens tissue paper and porcine liver tissue are demonstrated, illustrating a viable scanning approach for endomicroscopy in MIS.**

***Index Terms*—Endomicroscopy, optical biopsy, medical robotics, image mosaicing**

I. Introduction

With the development of minimally invasive approaches to surgery, such as single port surgery [1-2] and natural orifice transluminal endoscopic surgery (NOTES) [3-5], flexible endoscopes offer further scope for reducing access trauma and invasiveness. NOTES has also been developed as a minimally invasive approach to diagnostic laparoscopy [6-9]. However, it is currently necessary to take invasive biopsies if high-resolution tissue imaging is needed, such as for the identification of tumour margins.

In recent years, providing *in situ*, *in vivo* functional imaging of the exposed tissue surface has become an important research topic. This can further benefit minimally invasive surgery (MIS) by providing tissue detection, labelling, and targeting both at macro and cellular levels. Fluorescence confocal endomicroscopy [10], a cellular scale endoscopic imaging technique, could allow real-time assessment of tumour margins. In fluorescence confocal endomicroscopy, tissue is stained with a fluorescent contrast agent such as acriflavine hydrochloride or sodium fluorescein. A coherent fibre imaging bundle then relays a scanning laser pattern to the tissue and collects fluorescent signal. This allows optically sectioned images to be assembled, making it possible to image thick tissue *in vivo*. A number of groups have investigated the applications of confocal endomicroscopy, which, following application of a contrast agent, can allow the detection of disruption in the pit pattern in the colon, reveal microvasculature in sessile polyps, and highlight intestinal metaplasia in Barrett's Oesophagus [11]. pCLE is also used for assessment of indeterminate biliary strictures [12], in the lung [13], and can provide excellent sensitivity and specificity to common forms of cancer [14].

The development of confocal endomicroscopy provides the option of intraoperative optical biopsy, avoiding the risk of organ and tissue damage from standard tissue biopsy, and providing tissue information for real time diagnosis. However, the field-of-view for these devices is small (typically 0.2 to 0.7 mm). Although the effective coverage can be increased by mosaicing [15-17], this is difficult to achieve manually. This has led to the development of mechanical scanning devices for endomicroscopy. Several research groups have focused studies on high-accuracy industrial robot assisted scanning [18, 19]. The limitation of using a cooperative robotic arm is the difficulty of adapting a complex robot to clinical use. Some articulated robots have been developed for manipulation of endomicroscopy probes [20-23]. However, these devices are comprised of long, rigid shafts that can't approach the target in deep areas of the body in a flexible manner.

Several groups have developed flexible manipulators with a wide curve. For example, Ikuta et al. developed a micromanipulator to approach inaccessible regions [24]. Other flexible manipulators have also been developed, such as shape memory alloys (SMAs) robots [25], biomimetic untethered robots [26, 27], and twisted bundled tube locomotive device [28]. Moreover, some of the NOTES platforms such as EndoSAMURAI [29], direct drive endoscopic system (DDES) [30], and Flex Robotic System [31] have addressed many requirements for NOTES including triangulation, dexterity and platform stability issues. However, since most of these flexible instruments use wire-driven mechanism, they often suffer hysteresis problems. They thus cannot provide a robust and accurate tip-scanning trajectory at the distance scales required for endomicroscopy.

This application therefore requires a new flexible device which is capable of precise scanning over a large area of tissue,

This work was supported by EPSRC grant EP/IO27769/1: SMART Endomicroscopy.

Siyang Zuo is with the Key Laboratory of Mechanism Theory and Equipment Design of Ministry of Education, Tianjin University, Tianjin 300072, China (email: siyang_zuo@tju.edu.cn)

Michael Hughes and Guang-Zhong Yang are with the Hamlyn Centre for Robotic Surgery, Imperial College London, SW7 2AZ, London, UK (email: m.hughes@imperial.ac.uk, and g.z.yang@imperial.ac.uk).

accessed by a flexible route, with a simple and compact mechanical design. This paper proposes such a novel flexible scanning device for large area optical biopsy is. The flexible scanning device could also be combined with a NOTES platform or used in laparoscopic surgery. The features of the system are:

1. The flexible shaft of the device makes it possible to perform endomicroscopy in deep and narrow sites of the body, where it is difficult to perform minimally invasive surgery. The flexible body allows the device to be inserted without damaging the surrounding tissues.
2. The scanning mechanism adopts an elegant structure for practical clinical usage. A flexible concentric tube scanning structure is used to enable a robotized scanning motion at the tip, which can achieve various scanning trajectories.
3. A flexible concentric tube structure allows the driver source to be placed outside of the body, which enhances the safety of the system because there is no electrical current running in the body.
4. Because of the simple structure of the device, the scanning motion at the tip is easy to control via the motors. The surgeon only needs to push a 'start' button, and the scanning device can scan the target surface automatically.

In addition, the paper presents a detailed mechanical performance analysis of the scanning structure. Results from lens tissue paper and porcine liver tissue are demonstrated, illustrating a viable scanning approach for endomicroscopy.

II. Methods

A. Mechanical design

The proposed scanning mechanism incorporates a central channel for passing through a fibre imaging bundle for endomicroscopy. The distal structure consists of the tip and base frames, a pin joint, a spur gear link, a rotation gear, a flexible outer tube, and a flexible inner tube (**Fig. 1(A)**). The flexible inner and outer tubes are coaxially located and able to rotate independently. The flexible tubes are required to have excellent torque transmission efficiency to provide bending and rotating motions. The spur gear and rotation gear are in contact with each other in order to actuate the bending motion. The base frame and flexible outer tube are fixed together, while the rotation gear is fixed to the flexible inner tube. The scanning motion is then driven by control of the flexible inner and outer tubes. In our mechanical design, the flexible inner tube rotation angle α, the flexible outer tube rotation angle β, and tip bending angle φ are related by (1).

The proposed scanning mechanism has the ability to scan several trajectories, such as linear scans, concentric circles and spiral scans, by combining bending and rotating motion of the tip. For example, a spiral trajectory can be achieved by rotating the flexible inner and outer tubes simultaneously at varying angular velocities. The radial position h in xy dimensions can be determined by the relation between the tip frame length H and tip bending angle φ by (2). The radial position h, together with the Flexible outer tube rotation angle β, provides a spiral trajectory (**Fig. 1(B)**).

$$\varphi = \frac{R}{r}(\beta - \alpha) \tag{1}$$

$$h = Hsin(\frac{R}{r}(\beta - \alpha)) \tag{2}$$

B. Flexible scanning prototype

The scanning device system is shown in **Fig. 2 (A)**. The flexible scanning device consists of a scanning distal end for local scanning and approach-route selection, and a flexible shaft. The device has a maximum outer diameter of 6 mm and the length of the section which can be inserted into the patient is 300 mm (**Fig. 2 (B)**). In addition, the prototype is equipped with one 2.1 mm diameter central channel, through which the endomicroscope probe can be passed (**Fig. 2 (C)**).

The flexible inner and outer tubes are placed concentrically and driven by two high-resolution brushless DC-servomotors equipped with gear heads and Hall effect sensors (1226 E 012 B K1855, Faulhaber SA, Germany) (Fig. 2(D)). We utilized Helical Hollow Strand (HHS) tube as the driven tube, which is a medical grade wire (stainless steel). We used it to transmit torque and pushing forces due to its exceptional whip free characteristics and high resistance to kinks. There is also a 0.8 mm clearance between the inner and outer tubes which enables the system to transfer rotation independently and further minimizes internal friction. The backlash of the gears was minimized to an acceptable level by the inner HHS tube working as a spring to engage the rotation gear against the spur

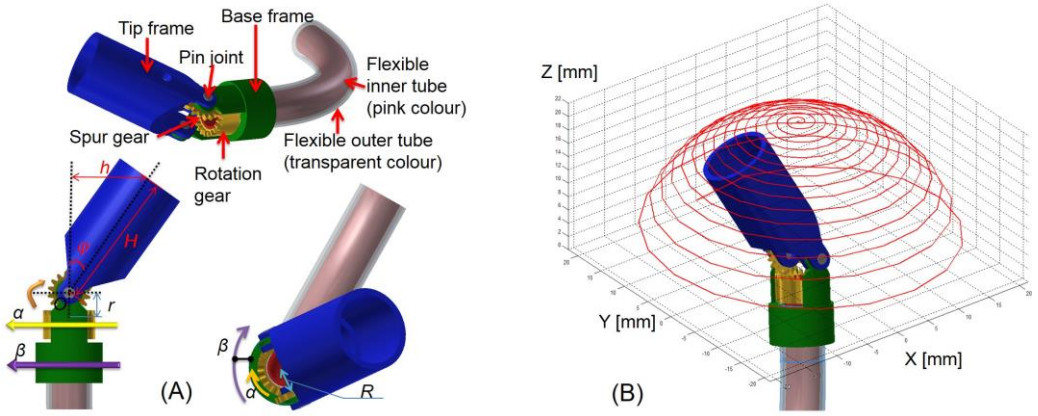

Fig. 1. Scanning mechanism, (A) transforming rotational motion of the Flexible outer and inner tubes to a scan motion of the distal end. (B) Spiral trajectory of the distal end.

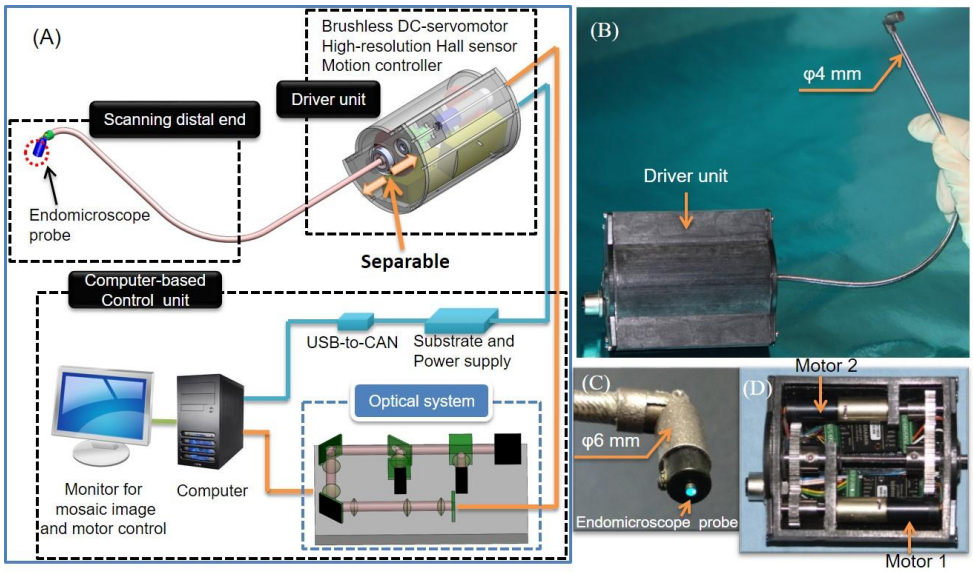

Fig. 2. Flexible scanning device. (A) System configuration of scanning device. (B) Prototype of the flexible scanning device. (C) Enlarged view of distal end with an endomicroscope probe. (D) Details of the driver unit with rotation gear, brushless DC-servomotors, gear head and Hall sensor.

gear link. Rotation gears are used for translating the rotation of the motors to the inner and outer tubes. The positional feedback control is achieved by Hall effect sensors. The probe tip velocity can be maintained approximately constant by control of the motors during scanning. For cleaning and sterilization reasons, the insertion parts of the scanning device can be separated from the driver unit. The commands to the motors are generated in Labview from a standard PC. In this custom-made interface, several parameters including the linear velocity of the probe, the required number of turns in the spiral or circle, and the radial spacing between turns are entered in advance. Then the scanning device can scan the target surface automatically once initiated. The actual signal output of the motor, including rotation speed and rotation angle, as well as the effective scan speed and radial position, are displayed and recorded.

C. Control algorithms

A spiral trajectory was adopted here as an example since it is an effective means of covering a scan area. For a spiral trajectory, the parameters include the linear velocity of the probe V_{linear}, and the loop spacing Δh. The parameters R, r and Δh are shown in Fig. 1. V_{linear} is given by (3).

$$V_{\text{linear}} = \frac{H\sin(\varphi_t)W_{m2t}}{\mu} \tag{3}$$

where μ is the gear ratio and W_{m2t} is the angular velocity of Motor 2.

Given a trajectory $x = Hsin\theta_t cos\varphi_t, y = Hsin\theta_t sin\varphi_t, z = Hcos\varphi_t$, We note that the length L_t of a spiral can be calculated by (4).

$$L_t = \int_0^t \sqrt{\dot{x}^2(t) + \dot{y}^2(t) + \dot{z}^2(t)} \tag{4}$$

Here, t is the scanning time.

Although the scanning device has a large hemispherical working space (20 mm in radius), a practical scanning target would only require scanning over a small range of bending angles of the scanning tip to avoid loss of tissue contact. The following equations apply in the limit of small bending angles which is appropriate when we are dealing with a small area scanning compared to the full hemi-spherical surface. This scanning device is targeted towards generation of a mosaic which is around 5 mm in diameter. This is a significant increase in area coverage compared to the field-of-view of the probe that is only around 0.5 mm in diameter.

A good approximation of the spiral parameters (length and radius) can be obtained from (5) and (6) if the loop spacing Δh is small compared to the mosaicing diameter. Here, h is the radius of the final point of the spiral. This approximate formula can be derived by considering a series of $(h/\Delta h)$ concentric circles with an average radius of $h/2$ and an average circumference of πh. The total length of the concentric circles, and to a good approximation the equivalent spiral, is given by:

$$L \approx \frac{\pi h^2}{\Delta h} \tag{5}$$

and hence:

$$h \approx \sqrt{\frac{\Delta h \cdot \mathrm{L}}{\pi}} \tag{6}$$

To have an idea of the error introduced by the approximate formula, the following is given as an example. Suppose the targeted scanning area is 5 mm in diameter ($h = 2.5mm$) and the loop spacing, $\Delta h = 0.5\ mm$. With the exact formula (4), we get $L = 39.57\ mm$. With the approximate formula (5), we get $L = 39.27\ mm$. The difference is only 0.3 mm over 39.57 mm, an error of 0.75 %, making this approximation suitable for calculation of length for simplicity.

It was found experimentally that a shift of 40 μm between images was necessary to ensure consistent mosaicing. Given the imaging frame rate of 10 fps, a maximum acceptable tangential velocity of 0.4 mm/s was selected. The frame overlap, Δp, is given by (7).

$$L_t = \Delta p \cdot F \cdot t \quad (7)$$

where t is the scanning time and F is the frame rate. Then the mosaicing diameter D_{1t} can be determined by (8).

$$D_{1t} \approx 2 \cdot \sqrt{\frac{\Delta h \cdot \Delta p \cdot F \cdot t}{\pi}} - \Delta h/2 \quad (8)$$

For the endomicroscopy system used in this study, the frame rate, F, is 10 Hz. The frame overlap, Δp, is chosen as 0.04 mm as discussed above. The relationship between mosaic diameter, scan time and loop spacing are illustrated in **Fig. 3.**

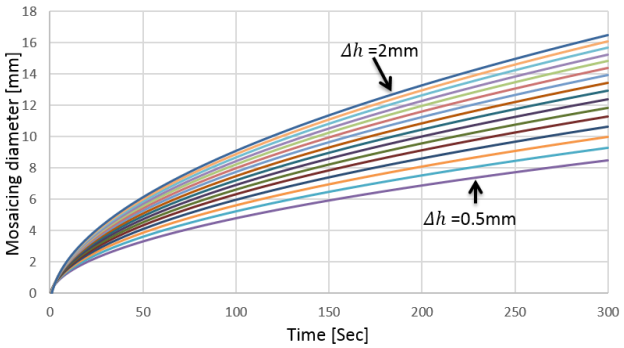

Fig. 3. The radial position that the device can scan over in a given time for values of the loop spacing Δh between 0.5 and 2 mm (the spacing is increased in 0.1 mm steps).

D. *Visualisation and image mosaicing*

The fibre-bundle used for this study was a Schott leached imaging bundle (P/N 1251343, SCHOTT North America, Inc.). It was used with an in-house laser scanning and image acquisition system for confocal endomicroscopy, similar to previously reported systems [10, 32]. This custom acquisition system allows a combination of imaging, mosaicing and scanner control for real-time use. For testing purposes, we used an offline mosaicing algorithm in Matlab. This algorithm estimates the x and y lateral shift and the rotation between successive frames using normalized cross-correlation. The rotation occurs because the 2D motion of the scanning device requires rotation of the distal tip.

The system was controlled by a Labview program, which reconstructed images based on the data acquired from the ADC board. The control scheme is summarised in **Fig. 4.** A Gaussian filter is adopted to remove the honeycomb-like structure arising from the discrete fibre bundle cores. Background corrections for each channel are acquired by averaging 10 frames. Finally, a window is applied to remove the edges of the fibre bundle and the image is auto-contrasted for live display to the user at 10 fps. An AVI video file can be recorded as necessary.

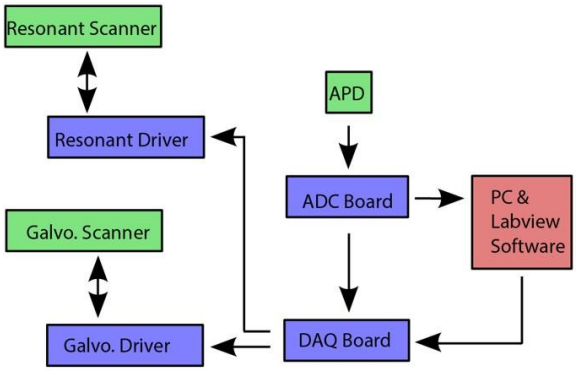

Fig. 4 Schematic of control scheme for laser scanning and synchronisation of image acquisition.

III. Results

A. *Mechanical performance evaluation*

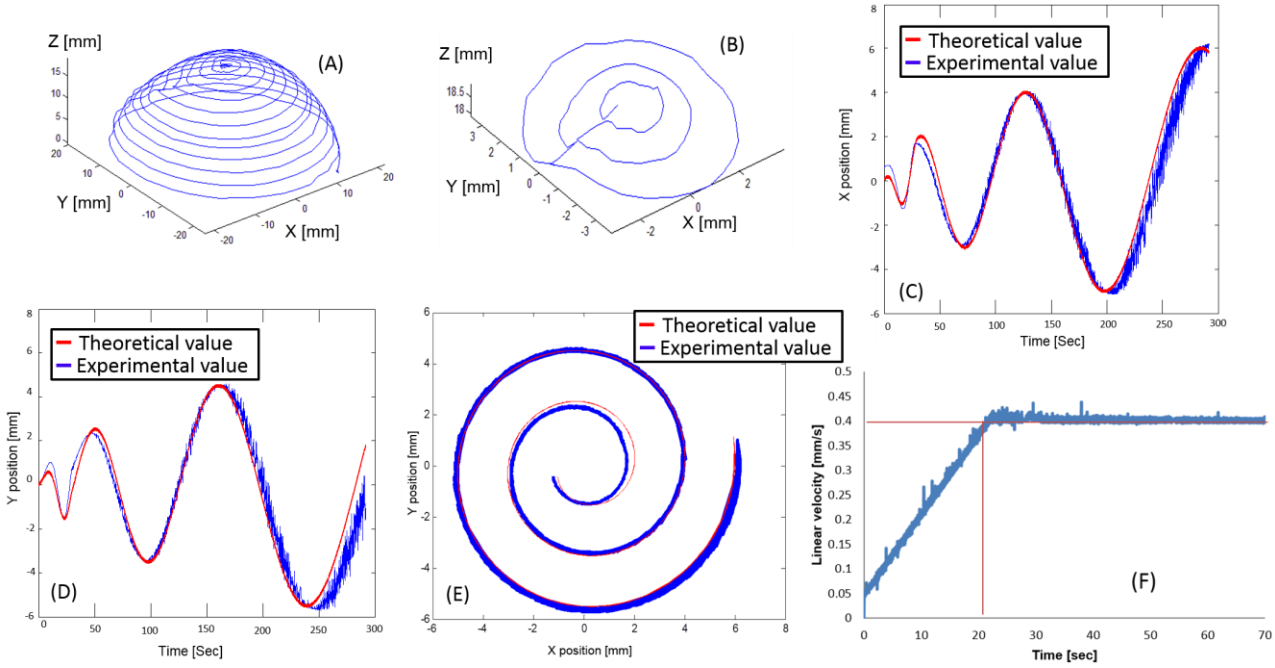

Fig. 5. Performance evaluation. (A) 3D trajectory of spiral scan, (B) 3D trajectory of concentric circle scan, (C) x position, (D) y position, (E) spiral trajectory, (F) the linear velocity of the tip of the scanning device.

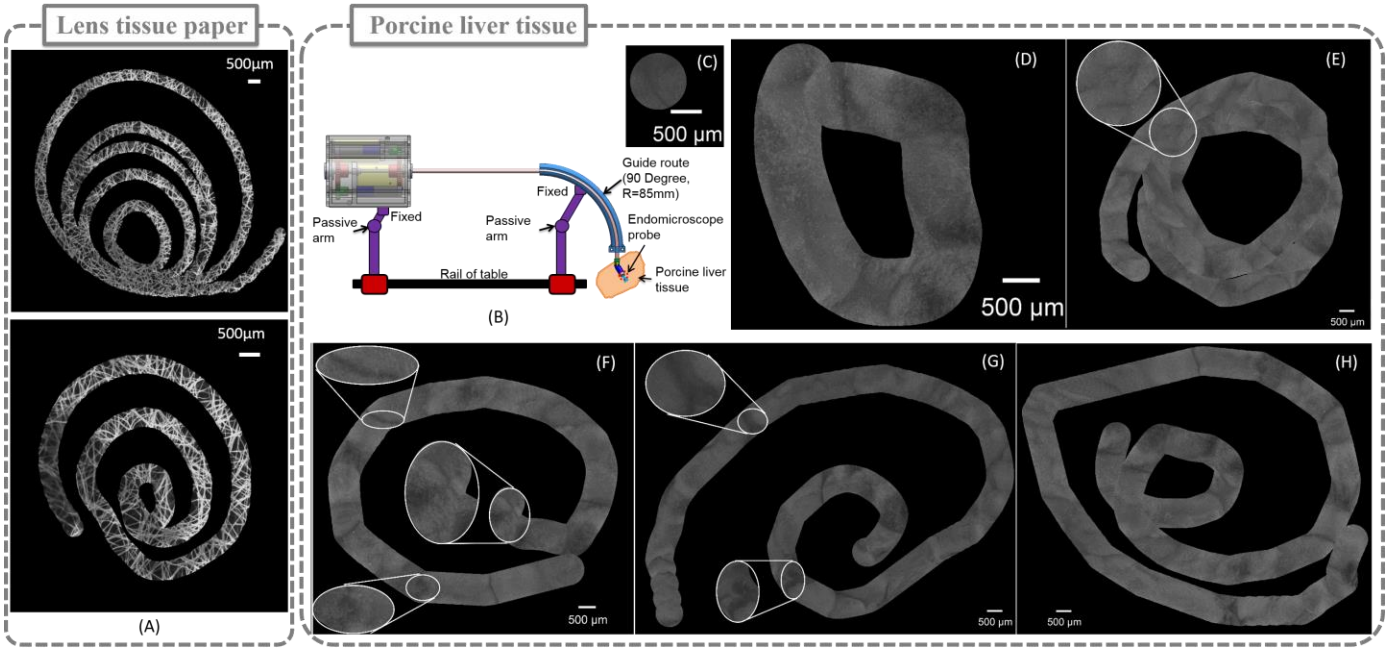

Fig. 6. Mosaicing valadation, (A) mosaic created from large area spiral scan over lens tissue paper stained with acriflavine; (A)-(H) imaging of porcine liver tissue stained with proflavine, showing (A) set up, (B) single point imaging, (C) small circle mosaic, (D) concentric circle mosaic, (E) large circle mosaic, (F) and (G) large area spirals.

We first examined the characteristics of the 2-DOF scanning mechanism with or without the Schott leached imaging bundle using a digital video camera. We used grid paper with a pitch of 0.05 mm (the effective pixel size of the camera in object space) to confirm that the accuracy of the camera was sufficient to evaluate the bending angle. The maximum error on the x-axis was 1 pixel, while the maximum error on y-axis was 0.5 pixel. Measurements of repeatability were performed over five trials each of the bending and rotating mechanisms, testing the actual bending angles against target angles input from the computer (**Table 1**).

Table 1. Characteristics of the scanning motion measured by a camera (n=5).

Measurement item	Without fibre bundle	With fibre bundle
Bending range (°)	-89.11 to 90.35	-86.4 to 88.26
Repeatability of bending (°)	±0.71	±2.9
Tip bending accuracy (mm)	0.5	2.0
One circle rotational range(°)	0 to 360.43	
Repeatability of rotation (°)	±0.4	
Tip rotating accuracy (mm)	0.2	

We then evaluated the trajectory of the tip using an NDI Aurora Electromagnetic Tracking System (NDI Corp, CA). A mini electromagnetic sensor with 6 DOFs was attached to the tip of the scanning device, allowing its position to be measured. A Kalman filter was applied as a low pass filter to remove the noise of the position measurements from the EM tracker. The trajectories of the spiral and concentric circle scans are shown in **Fig. 5 (A) (B)**. **Figs. 5(C) (D)** show the experimental and theoretical x, y positions, while the spiral trajectory is shown in **Fig. 5(E)**. We calculated the theoretical values from motor outputs. The linear velocity of a scan is plotted in **Fig. 5 (F)**. The tip linear velocity can be controlled to maintain a constant speed, typically 0.4 mm/s. We also measured the generated force using a digital force gauge. The bending and rotating forces were 0.7 N and 1.1 N respectively.

B. Mosaicing validation

We first scanned a spiral pattern over a piece of lens tissue paper stained with acriflavine. The scanning device was attached to a passive arm during the experiment and the spacing between loops of the spiral was set to approximately 1 mm. The resulting mosaic is shown in **Fig. 6 (A).** The results show that the scanning device could maintain almost constant tissue contact when scanning over a large area. There was distortion and unbalance in the mosaics, possibly due to deformation of the tissue paper during scanning. The deformation affects repeatability, but we were able to extract mosaics covering significant areas.

We scanned the porcine liver surface after taking a curved approach route (**Fig. 6 (B)**). The resulting mosaics are shown in **Fig. 6 (C) - (H)**. The outer and inner diameters of the circle area are approximately 8 mm and 3.6 mm respectively in **Fig. 6 (E)**. The circle mosaics, which are approximately 3.1 mm and 7.1 mm in diameter, are shown in **Fig. 6 (D) and (F)** respectively. A non-overlapping spiral pattern is shown in **Fig. 6 (G) and (H)**. The diameter of the spiral is approximately 10 mm and the spacing between loops of the spiral was set to approximately 2 mm. The trajectories are not perfect circles or spirals, most likely due to a combination of tip scanning inaccuracy when under load, mosaicing errors and deformation

of the scanned surface. Nevertheless, these image mosaics could allow for improved global appreciation of the tissue morphology when compared with individual images or small, manual mosaics.

IV. Discussion

The spiral workspace of the bending distal end (**Fig. 5(A)**) shows that the distal end can cover a large area with a radius of 20 mm. The distal end achieved high bending and rotating repeatability of ±0.71 ° and ±0.4 ° respectively. The bending range of the distal end is between -86.4 ° to 88.26 ° with a leached fibre bundle, which is a sufficient bending range for a large area scan. The bending range with a fibre bundle was a little less than without a fibre bundle because of the bundle's restoring force. However, this difference was very small and will not affect scanning maneuverability. With the fibre bundle, the positional errors at the tip are 2.0 mm (from bending motion) and 0.2 mm (from rotational motion). The positioning accuracy should be acceptable for larger field-of-view probes and large spiral or circle trajectories, but, for small field-of-view probes, large errors are likely to appear in the mosaics. Nevertheless, this still allows visualisation of a large area and may be satisfactory for diagnosis purpose.

The bending and rotating forces are 0.7 N and 1.1 N respectively. Stable images can be obtained when the tip contact force is between 0.1 N and 0.5 N [38, 39], and thus the achieved force makes it possible to carry out scanning with stable images. The trajectory experiment with the NDI Aurora Electromagnetic Tracking System showed that the distal end achieves a spiral and concentric circle scanning motion in 3D space. It took almost 20 seconds to reach the targeted linear velocity of 0.4 mm/s.

Depending on the shaft bending angle, the internal and external friction could affect image mapping. To an extent this problem is unavoidable, as for any flexible tube-based driven method, the complex shape of the shaft and friction of the driven structure will result in inaccurate image mapping. To minimize this negative effect, we utilized an HHS tube as the driven shaft. PTFE coatings can be used to enhance the lubricity of both internal and external movements. We can also use a PTFE guiding tube to cover the outer HHS tube to reduce the friction between the tube and tissues. Furthermore, the HHS tube can be manufactured in multiple layers in order to provide better control. Therefore, the friction between the flexible tubes could be low, resulting in a smooth rotation transmission and image scanning. In some small cavities inside the human body, the helical mesh structure of the outer tube can also provide a screw-like motion to facilitate insertion by rotating the outer tube.

One particular issue of the gear-based systems is backlash. However, backlash primarily occurs when changing the rotational direction of the gears. It therefore affects trajectories which bend back and forth, but there is little backlash during one-way bending such as spiral trajectories. Hence, it is easy to reduce the backlash because only one pair of specially-designed gears is adopted. In future, compensation and predictive control algorithms could improve the robustness of tip motion, and need to be further studied.

The flexible shaft of the scanning device makes it possible to enter deep and narrow areas of the human body. The minimum bend radius of the flexible shaft is 45 mm. This radius is sufficient for maneuvers around large organs such as the liver. Using the bending motion of the distal end, the flexible scanning device could in future allow selection of the approach route, which could make insertion easier. Moreover, the flexible scanning device, combined with the NOTES platform's four-directional flexion, could allow the creation of an array of mosaics centered on user-specified points of interest.

The lens tissue paper and porcine liver tissue evaluations in this study show that the flexible scanning device has strong potential to enable stable imaging. By increasing the rigidity of the flexible outer and inner tubes, the torque transmission to the distal end will be smoother, which could result in more stable scan motion. It is necessary to choose suitable rigidity and flexibility of the flexible inner and outer tubes depending on the application.

For validation of this study, we implemented a simple cross-correlation based mosaicing algorithm. Because the position and angle of each frame is determined by comparing it with the previous frame, this method accumulates errors during the scan. When combined with deformation of the tissue due to the motion of the probe, this results in mosaics which do not appear to closely match the programmed trajectory. Instead, distorted mosaics such as those shown above are obtained. It is difficult to quantitatively evaluate and distinguish between errors caused by tissue deformation, mechanical inaccuracy and cumulative mosaicking errors. The mosaicing results do, however, confirm that the probe follows a trajectory approximately as planned. This could be improved by integrating a more complex mosaicing algorithm that takes account of cumulative errors and tissue deformation. For example, mosaicing algorithms that do not assume rigid transformations can be used for correction of distortions due to tissue deformation [33]. These algorithms could be adopted for retrospective analysis. This may need to be run offline due to the associated computational complexity.

To control the scanning trajectory of the probe while accounting for tissue deformation, visual servoing could also be used. For example, Rosa et al. have used a robotic arm to generate a mosaic with consideration of tissue deformation [18]. Some studies have also looked at micro-optical assemblies such as fisheye lenses for the tip of the endomicroscope which have the potential to create larger effective overlaps of the viewing area during probe actuation, although this work is relatively immature.

The scanning device could be combined with shape-lockable platforms, such as direct drive endoscopic system (DDES, developed by Boston Scientific, MA) [30], rigid and flexible outer sheaths [34-35], or the Incisionless Operating Platform (IOP, developed by USGI Medical, CA) [36-37]. These NOTES platforms are equipped with working channels that are more than 6 mm in diameter. Thus, the scanning device could reach the target through the working channel of the NOTES platform. During a NOTES procedure, the surgeon would perform an initial visual inspection using the endoscopic camera view, and then either apply a topical fluorescent contrast agent to the suspected area by a tube inserted through

working channel of the NOTES platform, or inject a systemic contrast agent (fluorescein). The scanning device would then be inserted through the working channel, moved to the target area by the NOTES platform under image guidance, and deployed against the target tissue. This would allow real-time evaluation of the tissue microstructure without the need for invasive biopsy. In particular, the device could be used for transrectal and transvaginal NOTES, because the approach is suitable for short, gentle curves.

In laparoscopy, the device could be directly inserted through the abdominal ports on the patient. The laparoscope could then be used to guide the scanning device to reach the target and perform scanning procedures. In both cases, images could be streamed from the endomicroscope and overlaid live onto the surgeon's view. The 2D mosaics could also be fused into a 3D stereo reconstruction of the surgical scene from laparoscope, thus providing intuitive visualisation and fusion of the multi-scale images.

At the start of each scan, we manually adjusted the motors to ensure the scanning tip returned to a straight condition using a set up tube, and then made a re-initialization of the motors. In practice, the start-point for a scan may need to be from a different position, to accommodate the possible access route and available workspace. In this case, firstly, the tip would need to be bent until a good quality of the tissue image was obtained, implying that proper tissue contact has been achieved. Parts of the hemisphere could then be scanned using raster trajectories.

V. Conclusion

In conclusion, we have developed a new flexible scanning device for endomicroscopy in deep and narrow areas in the human body. The experimental results showed that the flexible scanning device could follow a curved path with a suitable radius of curvature and that it can scan over a local area. We have demonstrated the potential to provide a much larger field-of-view for optical biopsy than conventional endomicroscopy. This could offer the surgeon more comprehensive information than single-point imaging or short manual mosaics, greatly improving the prospects for intraoperative *in situ* margin evaluation.

Reference

[1] P. Rao, S. Rao, A. Rane´, F. Bondaio, "Evaluation of the R-port for single laparoscopic port procedures (SLAPP): a study of 20 cases," Surg. Endosc, vol. 22, Suppl 1, pp. S279, 2008.

[2] F.H. Remzi, H.T. Kirat, J.H. Kaouk, D.P. Geisler, "Single-port laparoscopy in colorectal surgery," Colorectal Dis, vol.10, no.8, pp. 823–826, Epub 5 August 2008.

[3] D.Rattner,A. Kalloo,"ASGE/SAGES Working Group on Natural Orifice Translumenal Endoscopic Surgery," J.Surg. Endosc, vol.20, pp. 329–333, 2006.

[4] J. Marescaux, B. Dallemagne, S. Perretta, A. Wattiez, D. Mutter, D. Coumaros,"Surgery without scars:report of transluminal cholecystectomy in a human being,"J.Arch. Surg, vol.142, pp. 823–826, 2007.

[5] J. P. Pearl, J. L. Ponsky, "Natural orifice translumenal endoscopic surgery: a critical review,"J. Gastrointest. Surg, vol.12, pp. 1293–1300, 2008.

[6] J. Hazey, V. Narula, D. Renton, K. Reavis, C. Paul, K. Hinshaw, P. Muscarella, E. Ellison, W. Melvin,"Natural-orifice transgastric endoscopic peritoneoscopy in humans: initial clinical trial, " Surg Endosc, vol.22, pp. 16–20, 2008.

[7] R .P. Voermans, B. Sheppard, M .I. van Berge Henegouwen, P. Fockens, D .O. Faigel, "Comparison of transgastric NOTES and laparoscopic peritoneoscopy for detection of peritoneal metastases,"Ann Surg, vol.250, pp. 255–259, 2009.

[8] K. Steele, M .A. Schweitzer, J .Lyn-Sue, S .V. Kantsevoy, "Flexible transgastric peritoneoscopy and liver biopsy:a feasibility study in human beings (with videos),"Gastrointest Endosc, vol.68, pp. 61–66, 2008.

[9] R .P. Voermans, M .I. van Berge Henegouwen, W.A. Bemelman, P. Fockens, "Feasibility of transgastric and transcolonic natural orifice transluminal endoscopic surgery peritoneoscopy combined with intraperitoneal EUS,"Gastrointest Endosc, vol.69, pp. e61–e67, 2009.

[10] J. M. Jabbour,M. a. Saldua, J. N.Bixler,K.C.Maitland, "Confocal Endomicroscopy:Instrumentation and Medical Applications," Annals of biomedical engineering, 2011.

[11] A. Meining, M. Bajbouj, S. von Delius, and C. Prinz, "Confocal Laser Scanning Microscopy for in vivo Histopathology of the Gastrointestinal Tract," Arab Journal of Gastroenterology, vol.8, pp. 1–4, 2007.

[12] C .S. Loeser, et al, "Confocal endomicroscopic examination of malignant biliary strictures and histologic correlation with lymphatics," J Clin Gastroenterol, vol.45, no.3, pp. 246–52, 2011.

[13] R .C. Newton, et al, "Imaging parenchymal lung diseases with confocal endomicroscopy," Respiratory Medicine, vol.106, no.1, pp.127–137, 2012.

[14] P. Su, et al, "Efficacy of confocal laser endomicroscopy for discriminating colorectal neoplasms from non-neoplasms:a systematic review and meta-analysis,"Colorectal Disease, vol.15, no.1, pp. e1–e12, 2013.

[15] N. Ayache, T. Vercauteren, G. Malandain, F. Oberrietter, N. Savoire, and A. Perchant, "Processing and mosaicing of fibered confocal images," in Microscopic Image Analysis with Applications in Biology, 2006.

[16] V. Becker, T. Vercauteren, C .H. von Weyhern, C. Prinz, R .M Schmid, and A. Meining, "High-resolution miniprobe-based confocal microscopy in combination with video mosaicing (with video)," Gastrointest. Endosc, vol.66, no.5, pp. 1001–1007, 2007.

[17] N. Bedard, T. Quang, K. Schmeler, R. Richards-Kortum, T. Tkaczyk, "Real-time video mosaicing with a high-resolution microendoscope," Biomedical Optics Express 3, pp. 2428–35, 2012.

[18] B. Rosa, et al, "Building large mosaics of confocal endomicroscopic images using visual servoing," IEEE transactions on biomedical engineering, vol.60, pp. 1041–1049, 2013.

[19] P. Giataganas, V. Vitiello, V. Simaiaki, E. Lopez, and G. Z. Yang, "Cooperative in situ microscopic scanning and simultaneous tissue surface reconstruction using a compliant robotic manipulator," in IEEE International Conference on Robotics and Automation (ICRA 2013), pp. 5378-5383, 2013.

[20] M. Burkhardt, T. Soper, W. J. Yoon, and E. Seibel, "Controlling the trajectory of a flexible ultrathin endoscope for fully automated bladder surveillance," IEEE/ASME Trans. Mechatronics, vol. 19, no. 1, pp. 366– 373, 2014.

[21] X. Ye, Y. Gong, and J. Yoon, "Development of multi-segment steering mechanism and 3D panorama for automated bladder

surveillance system," IEEE/ASME Trans. Mechatronics, vol. 21, no. 2, pp. 993-1003, 2016.
[22] M. S. Erden, et al, "Conic-Spiraleur: A Miniature Distal Scanner for Confocal Microlaparoscope," IEEE/ASME Trans. Mechatronics, vol.19, no.6, pp. 1786–1798, 2014.
[23] S. Zuo, M. Hughes, and G.-Z. Yang, "Novel Balloon Surface Scanning Device for Intraoperative Breast Endomicroscopy," Annals of biomedical engineering, vol.44, no.7, pp. 2313–2326, 2016.
[24] K. Ikuta, K. Sasaki, K. Yamamoto, T. Shimada, "Remote Microsurgery System for Deep and Narrow Space - Development of New Surgical Procedure and Microrobotic Tool," In: T. Dohi , R. Kikinis, (eds.) MICCAI 2002. LNCS, vol. 2488, pp. 163–172. Springer, Heidelberg, 2002.
[25] D. Hwang and T. Higuchi, "A rotary actuator using shape memory alloy (SMA) wires," IEEE/ASME Trans. Mechatronics, vol. 19, no. 5, pp. 1625–1635, Oct. 2014.
[26] F. Z. Temel, A. G. Erman, and S. Yesilyurt, "Characterization and modeling of biomimetic untethered robots swimming in viscous fluids inside circular channels," IEEE/ASME Trans. Mechatronics, vol. 19, no. 5, pp. 1562– 1573, Oct. 2014.
[27] T. Xu, G. Hwang, N. Andreff, and S. Regnier, "Modeling and swimming property characterizations of scaled-up helical microswimmers," IEEE/ASME Trans. Mechatronics, vol. 19, no. 3, pp. 1069–1079, Jun. 2014.
[28] T. Takayama, H. Takeshima, T. Hori and T. Omata, "A twisted bundled tube locomotive device proposed for in-pipe mobile robot", IEEE/ASME Trans. Mechatronics, vol. 20, no. 6, pp. 2915-2923, 2015
[29] G.O. Spaun, B. Zheng, L.L. Swanstrom, "A multitasking platform for natural orifice translumenal endoscopic surgery (NOTES): a benchtop comparison of a new device for flexible endoscopic surgery and a standard dual-channel endoscope", Surg Endosc, vol. 23, pp. 2720-2727, 2009
[30] C.C. Thompson, M. Ryou, N.J. Soper, E.S. Hungess, R.I. Rothstein, L.L. Swanstrom, "Evaluation of a manually driven, multitasking platform for complex endolumenal and natural orifice translumenal endoscopic surgery applications (with video)," Gastrointest Endosc, vol. 70, no. 1, pp. 121-125, 2009
[31] M. Remacle, V.M.N. Prasad, G. Lawson, L. Plisson, V. Bachy, S. Van der Vorst, "Transoral robotic surgery (TORS) with the Medrobotics Flex™ System: first surgical application on humans," Eur Arch Otorhinolaryngol, vol. 276, pp. 1451–1455, 2015
[32] G. Goualher, A. Perchant, M. Genet, C. Cav, B. Viellerobe, B. Abrat, and N. Ayache,"Towards optical biopsies with an integrated fibered confocal fluorescence microscope,"in Medical Imaging Computing and Computer Assisted Intervention (MICCAI), 2004.
[33] T. Vercauteren, A. Perchant, G. Malandain, X. Pennec, and N. Ayache, "Robust mosaicing with correction of motion distortions and tissue deformations for in vivo fibered microscopy," Medical image analysis 10, no. 5, pp. 673-692, 2006.
[34] Zuo S, Masamune K, Kuwana K et al. Nonmetallic rigidflexible outer sheath with pneumatic shapelocking mechanism and double curvature structure. Med Image Comput Comput Assist Interv –MICCAI 2012, Lecture Notes in Computer Science 2011; 6891:169–177
[35] Zuo S, K Iijima, T Tokumiya, K Masamune. Variable stiffness outer sheath with ''Dragon skin'' structure and negative pneumatic shape-locking. Int. J. Comput. Assist. Radiol. Surg. 2014; 9(5):857–865
[36] Swanström L, Swain P, Denk P. Development and validation of a new generation of flexible endoscope for NOTES. Surg Innov 2009; 16: 104-110.
[37] Horgan S, Thompson K, Talamini M, Ferreres A, Jacobsen G, Spaun G, et al. Clinical experience with a multifunctional, flexible surgery system for endolumenal, single-port, and NOTES procedures. Surg Endosc 2011; 25(2):586-592.
[38] W. Latt , R. Newton , M. Visentini-Scarzanella , C. Payne , D. Noonan , J. Shang and G. Z. Yang, "A hand-held instrument to maintain steady tissue contact during probe-based confocal laser endomicroscopy", IEEE Trans. Biomed. Eng., vol. 58, no. 9, pp.2694 -2703 2011.
[39] R. C. Newton , D. P. Noonan , C. Payne , J. Andreyev , A. Di Marco , M. V. Scarzanella , A. Darzi and G.Z. Yang, "Probe tip contact force and bowel distension affect crypt morphology during confocal endomicroscopy", Gut, vol. 60, pp.A12 -A13 2011.

Siyang Zuo received the M.Eng. and Ph.D. degrees in Information Science and Technology from the University of Tokyo, Japan, in 2009 and 2013, respectively. He is currently a professor in the Key Laboratory of Mechanism Theory and Equipment Design of Ministry of Education, School of Mechanical Engineering, Tianjin University, China. His research interests include medical robotics and imaging techniques.

Michael Hughes received his PhD in Physics from University of Kent, U.K, in 2009. He is a Hamlyn Fellow at the Hamlyn Centre, Imperial College London. His current research mainly focuses on new ways of building thin, flexible endoscopic and needle microscopes.

Guang-Zhong Yang (S'90–M'91–SM'08–F'11) received his PhD in Computer Science from Imperial College London, U.K. He is the Director and co-founder of the Hamlyn Centre, and Deputy Chairman of the Institute of Global Health Innovation (IGHI), Imperial College London, London, U.K. Professor Yang's main research interests are in medical imaging, sensing and robotics.